Inorganic Chemistry
Article
Cite This: Inorg. Chem. 2018, 57, 15330−15340
pubs.acs.org/IC

Determination of Large Zero-Field Splitting in High-Spin Co(I) Clathrochelates

Joscha Nehrkorn,*[,†,‡,§,∥] Sergey L. Veber,[⊥,#] Liudmila A. Zhukas,[⊥,#] Valentin V. Novikov,[¶] Yulia V. Nelyubina,[¶] Yan Z. Voloshin,[¶] Karsten Holldack,[▽] Stefan Stoll,[‡] and Alexander Schnegg*[,§,∥]

[†]Department of Chemistry, Institute for Inorganic and Applied Chemistry, University of Hamburg, Martin-Luther-King-Platz 6, D-20146 Hamburg, Germany

[‡]Department of Chemistry, University of Washington, Box 351700, Seattle, Washington 98195-1700, United States

[§]Berlin Joint EPR Laboratory, Institut für Nanospektroskopie, Helmholtz-Zentrum Berlin für Materialien und Energie, Kekuléstr. 5, D-12489 Berlin, Germany

[∥]Max Planck Institute for Chemical Energy Conversion, Stiftstr. 34-36, D-45470 Mülheim an der Ruhr, Germany

[⊥]International Tomography Center, Siberian Branch of the Russian Academy of Sciences, Institutskaya str. 3a, 630090 Novosibirsk, Russia

[#]Novosibirsk State University, Pirogova str. 1, 630090 Novosibirsk, Russia

[¶]Nesmeyanov Institute of Organoelement Compounds, Russian Academy of Sciences, Vavilova str. 28, 119991 Moscow, Russia

[▽]Institut für Methoden und Instrumentierung der Forschung mit Synchrotronstrahlung, Helmholtz-Zentrum Berlin für Materialien und Energie, Albert-Einstein-Str. 15, D-12489 Berlin, Germany

Supporting Information

ABSTRACT: Zero-field splitting (ZFS) of three high-spin Co(I) (S = 1) clathrochelate complexes was determined by frequency-domain Fourier-transform THz-EPR (FD-FT THz-EPR). The following axial and rhombic ZFS values (D and E, respectively) were determined: $[N(n\text{-}Bu)_4]Co^{I}(GmCl_2)_3(BPh)_2$ (**1**, D/hc = +16.43(1) cm^{-1}, E/hc = 0.0(1) cm^{-1}), $[P(Me_2N)_4]$-$Co^{I}(GmCl_2)_3(BPh)_2$ (**2**, D/hc = +16.67(4) cm^{-1}, E/hc = 0.0(1) cm^{-1}), and $[P(C_6H_5)_4]Co^{I}(GmCl_2)_3(BPh)_2$ (**3**, D/hc = +16.72(2) cm^{-1}, E/hc = 0.24(3) cm^{-1}). Complementary susceptibility χT measurements and quantum chemistry calculations on **1** revealed hard-axis-type magnetic anisotropy and allowed for a correlation of ZFS and the electronic structure. Increased rhombicity of **3** as compared to **1** and **2** was assigned to symmetry changes of the ligand structure induced by the change of the counterion. **1** and **3** exhibited temperature-dependent ZFS values. Possible reasons for this phenomenon, such as structural changes and weak chain-like intermolecular antiferromagnetic interactions, are discussed.

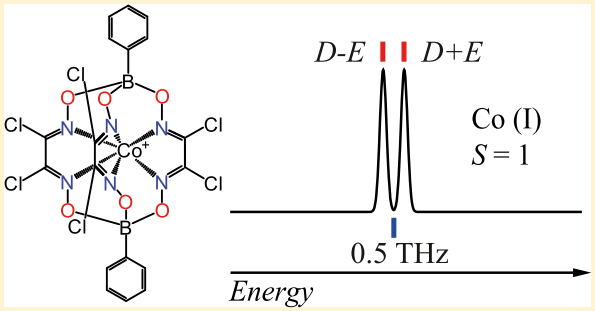

INTRODUCTION

Molecular nanomagnets (MNMs)[1] are emerging as prospective components for information storage,[2] spintronics,[3] quantum computing,[4] and magnetic refrigeration.[5] A key property of MNMs is their, oftentimes large, magnetic anisotropy, which arises from spin−spin and spin−orbit interactions.[6,7] The fascination for MNMs stems mainly from their magnetic properties that are of purely molecular origin, in contrast to conventional magnets where they arise from interactions over an extended network. However, intermolecular interactions (IMIs) might contribute[8] and would be essential for using MNMs as qubits for quantum computing or storage.[9] Effects of IMI on the magnetization dynamics were observed for several MNMs,[10−15] and various experimental methods were proposed to estimate the strength of IMIs.[16−27]

In this context, Co complexes attract significant attention. They oftentimes exhibit very large magnetic anisotropies and have been successfully used as building blocks in single-molecule magnets.[28,29] However, clear-cut correlations between the magnetic properties and the atomic and electronic structure are in their infancy.[15,30,31] Furthermore, studies have been in most cases dedicated to Co(II), but very little is known about their Co(I) counterparts.[32−39]

Herein, we studied spin ground-state energy splittings [zero-field splitting (ZFS)] of a series of Co(I) clathrochelate complexes. The $3d^8$ ion is found in a spin triplet (S = 1) ground state, which is less common than a spin singlet. In these

Received: September 19, 2018
Published: November 29, 2018

DOI: 10.1021/acs.inorgchem.8b02670
Inorg. Chem. 2018, 57, 15330−15340

complexes (see Scheme 1), Co(I) is coordinated by the six nitrogen atoms of three dichloroglyoxime fragments ($GmCl_2$),

Scheme 1. Anion of the Studied Co(I) Clathrochelates (Determined for 1)

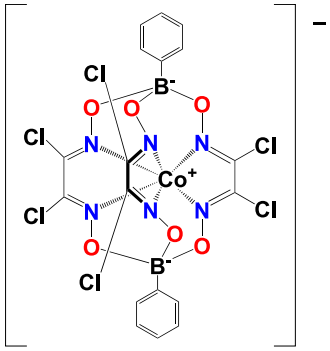

which form a three-dimensional caging ligand upon binding by two capping phenylboronic acid fragments (BPh), to give overall the clathrochelate ligand $[(GmCl_2)_3(BPh)_2]$. This ligand arrangement gives rise to a trigonal prismatic geometry and an orbitally nondegenerate ground state. The ligands fully encapsulate Co(I) in a protective cage and isolate it from the environment. This results in high chemical stability of these cage complexes (often called clathrochelates).[40−42] Along the studied series, the anion remains unaltered and the counterion was varied.

The ground-state energy levels of an isolated high-spin Co(I) with $S = 1$ exhibiting magnetic anisotropy can be described by the following spin Hamiltonian[1]

$$\hat{H} = D\left(\hat{S}_z^{\,2} - \frac{1}{3}\hat{\boldsymbol{S}}^2\right) + E(\hat{S}_x^{\,2} - \hat{S}_y^{\,2}) + \mu_B g \boldsymbol{B}_0 \cdot \hat{\boldsymbol{S}} \quad (1)$$

The first and second terms represent axial and rhombic magnetic anisotropy, respectively, that split the energy levels already at zero magnetic field, resulting in ZFS. For mononuclear transition-metal ion MNMs, D and E are the major source of spin ground-state energy level splitting. However, as we will outline below, other contributions like IMI may influence these splittings. Therefore, in the present manuscript, we denote any spin ground-state splitting irrespective of its origin as ZFS. The third term describes the electron Zeeman interaction between the MNM and the external magnetic field $\boldsymbol{B}_0$, under the assumption of an isotropic g matrix.

The method of choice for measuring ZFS is electron paramagnetic resonance (EPR) using microwave frequencies ν_{MW} larger or comparable to the ZFS.[43] This, however, can be challenging, as the frequency needed is not known a priori and most EPR spectrometers are fixed-frequency devices. This issue is severe for integer S: often, no EPR absorption is observed in the accessible field range. Complexes that do not show EPR absorption in conventional X- and Q-band spectrometers have been previously referred to as "EPR silent". To lift this restriction, FD-FT THz-EPR was employed. This method is a powerful tool for determining ZFS of high-spin transition-metal ion complexes.[14,30,44−56] Frequency-domain EPR for an $S = 1$ spin system has the convenient property that both D and E can be directly read off from the zero-field spectrum, which contains two EPR lines centered at an energy of D and separated by $2E$ (a single line at D in the case of vanishing E).

Here, we used a combination of FD-FT THz-EPR, susceptibility measurements, and quantum chemistry calculations to accurately determine and rationalize the ZFS of a series of Co(I) clathrochelate complexes. The nature of the counter-ion had a subtle effect on D and E. Further, the observed ZFS showed a slight temperature dependence. We discuss the possible reasons for this phenomenon, including structural changes and weak chain-like intermolecular antiferromagnetic interactions.

EXPERIMENTAL SECTION

Synthesis. $[N(n\text{-}Bu)_4]Co^I(GmCl_2)_3(BPh)_2$ (**1**) was synthesized as described previously.[57] The Co(I) clathrochelate anion was isolated as a salt with the tetrabutylammonium cation $[N(n\text{-}Bu)_4]^+$. Briefly, the corresponding Co(II) clathrochelate and tetrabutylammonium bromide were dissolved in an acetonitrile/dichloromethane (3:1) mixture. An excess amount of silver powder was added to reduce the Co(II) ion, and the reaction mixture was stirred overnight under argon followed by recrystallization from dichloromethane. As the spectral properties (UV−vis, MS, and IR) of the complex were identical to those reported previously, we employed the superconducting quantum interference device (SQUID) magnetometry data (temperature dependence of magnetic susceptibility) from the original paper.[57] The clathrochelates $[P(Me_2N)_4]Co^I(GmCl_2)_3(BPh)_2$ (**2**) and $[P(C_6H_5)_4]$-$Co^I(GmCl_2)_3(BPh)_2$ (**3**) were synthesized as **1**, except that [P-

Table 1. Summary of the Experimental Conditions[a]

	1	2	3
sample amount (mg)	159	97	101
PE powder (mg)	103	100	100
pellet (mg)	253	170	188
reference (field dependencies)	33 K, 0 T	42 K, 0 T	2.4 K, 7 T
	(5 K, 0 T)	(2.4 K, 0 T)	(2.4 K, all $\boldsymbol{B}_0$)
	33 K, 0.5 T	33 K, 0.5 T	
	(5 K, all other $\boldsymbol{B}_0$)	(2.4 K, 0.5 T)	
		34 K, 3 T	
		(2.4 K, 1.5 and 3 T)	
reference (temperature dependencies)	44 K, 0 T	43 K, 0 T	7 T
spectral regions (in cm^{-1}) used for uncertainty estimation	11−15.5	11−13.5	11−14
	18.2−21	18.5−23	18−22

[a]The amount of the sample mixed with PE and the weight of the resulting pellet. Further, the temperature and magnetic field at which the reference spectrum was recorded. The conditions of the spectra for which the references were used are indicated in brackets. Finally, the spectral region used for the uncertainty estimation is given.

DOI: 10.1021/acs.inorgchem.8b02670
Inorg. Chem. 2018, 57, 15330−15340

$(Me_2N)_4]I$ and $[P(C_6H_5)_4]Cl$, respectively, were used instead of $[N(n\text{-}C_4H_9)_4]Br$.

Quantum Chemical Calculations. Quantum chemical calculations were performed with ORCA 4.0.1.2.[58] X-ray diffraction data of **1** were used as the initial structure for the geometry optimization with a nonhybrid PBE functional,[59] the scalar relativistic zero-order regular approximation,[60] and the scalar relativistically recontracted[61] version of the def2-TZVP basis set.[62] Ab initio CASSCF calculations were performed with the def2-TZVP basis set for all atoms, along with an auxiliary basis set formed using the autoaux command available in ORCA.[63] The active space for CASSCF calculations was chosen to consist of the 5 cobalt 3d-based molecular orbitals and 8 electrons (CAS(8,5)) with 10 triplet and 15 singlet electronic states taken into account. In all CASSCF-based calculations, scalar relativistic effects were accounted for by the second-order Douglas−Kroll−Hess procedure.[64−67] The converged wavefunctions were then subjected to N-electron valence perturbation theory to second order (NEVPT2) to account for dynamic correlation.[68−71] Temperature dependence of χT was calculated from the CASSCF/NEVTP2-derived energy levels of cobalt(I) clathrochelate using the approach described in ref 72.

FD-FT THz-EPR Experiments. The FD-FT THz-EPR data were acquired at the THz-EPR user-station of the electron-storage ring BESSY II. The setup is described in detail elsewhere.[53,73,74] For the FD-FT THz-EPR experiments reported herein, THz coherent synchrotron radiation (CSR)[75] was used as the broad band (4−50 cm^{-1}) excitation source. The radiation was transmitted by a quasi-optical evacuated transmission line through a Fourier transform infrared (FTIR) spectrometer (Bruker IFS 125, maximum experimental resolution: 0.0063 cm^{-1}). Experiments were performed with experimental resolutions of 0.025 cm^{-1} (temperature dependence of $\Delta_B A$ spectra of **3**) and 0.1 cm^{-1} (all other experiments). After passing through the spectrometer, the radiation was focused on the sample immersed in a superconducting magnet (Oxford Spectromag). The transmitted signal was detected by a bolometer detector and Fourier-transformed to yield frequency-domain EPR spectra. The samples (polycrystalline powder of the Co(I) clathrochelate mixed with polyethylene (PE) powder pressed to a pellet; amounts are summarized in Table 1) were mounted in the variable-temperature insert of the magnet. FD-FT THz-EPR, as an FTIR-based technology, requires the measurement of a reference spectrum. In the present work, two alternative strategies were employed to obtain reference spectra. $\Delta_T A$ spectra employ a spectrum measured at a higher temperature as the reference, whereas for $\Delta_B A$, the reference is measured at the same temperature but at a magnetic field of 7 T. $\Delta_{T,B} A$ spectra were obtained as $\Delta_{T,B} A = \log_{10}(I_{ref}/I_0)$, where I_{ref} is a reference spectrum and I_0 is the spectrum measured at the indicated conditions. The measurement conditions for the used reference spectra are summarized in Table 1. The uncertainty in the energy at which the maximum in $\Delta_{T,B} A$ is obtained based on the uncertainty in $\Delta_{T,B} A$. Therefore, the uncertainty of $\Delta_{T,B} A$ is estimated as the standard deviation of $\Delta_{T,B} A$ in spectral regions without magnetic transitions (summarized in Table 1). Subsequently, the uncertainty in energy was obtained as the energy at which $\Delta_{T,B} A$ is reduced by this standard deviation compared to the maximum.

RESULTS AND DISCUSSION

For **1**, the variable-temperature dc magnetic susceptibility χT (Figure 1) is 1.06 cm^3 $kmol^{-1}$ at 300 K, as expected for $S = 1$ ($\chi T \approx \frac{g^2 S(S+1)}{8}$ cm^3 $kmol^{-1}$ = 1.06 cm^3 $kmol^{-1}$ for $g = 2.06$). The dependence of χT on temperature (no changes upon cooling down to 50 K followed by a sharp drop as temperature is decreased further) is indicative of either significant antiferromagnetic interactions (on the order of a few cm^{-1}) or ZFS.

To discriminate between dominating antiferromagnetic couplings and ZFS as the source of the observed χT, we performed FD-FT THz-EPR. This allows for a direct determination of the ZFS with superior precision as compared to susceptibility measurements. FD-FT THz-EPR $\Delta_T A$ spectra of **1** measured at 5 K and at different magnetic fields are shown in Figure 2. At zero field, the spectrum exhibits a resonance at 16.43 cm^{-1}, which broadens and drastically changes its shape upon applying the magnetic field. Strong changes with the magnetic field indicate that this resonance is of a magnetic rather than of a dielectric origin.

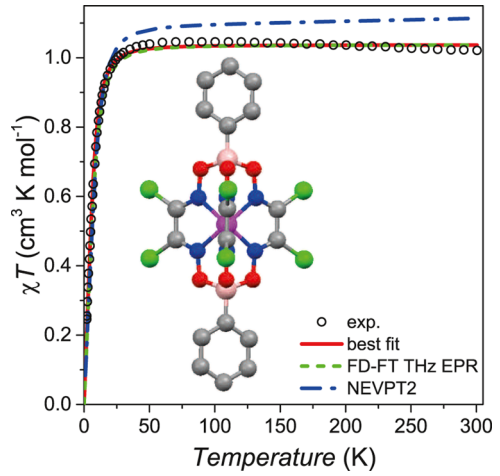

Figure 1. Variable-temperature dc magnetic susceptibility χT (black circles) of microcrystalline **1**.[57] The red solid and green dotted lines are simulations using eq 1 with D/hc = 14.4 cm^{-1}, E/hc = 0 cm^{-1}, and g = 2.036 (best-fit to χT) and D/hc = 16.43 cm^{-1}, E/hc = 0.0 cm^{-1}, and g = 2.0 (best-fit to FD-FT THz-EPR spectra). χT calculated from CASSCF/NEVPT2 results are shown as the blue dash-dotted line. The inset shows a ball-and-stick representation of the anion of the studied Co(I) clathrochelates. Co(I) ion: magenta, O: red, N: blue, Cl: green, C: gray, B: pink. H atoms are omitted for clarity. The pseudo-C_3 axis passes through B, Co(I), and B atoms.

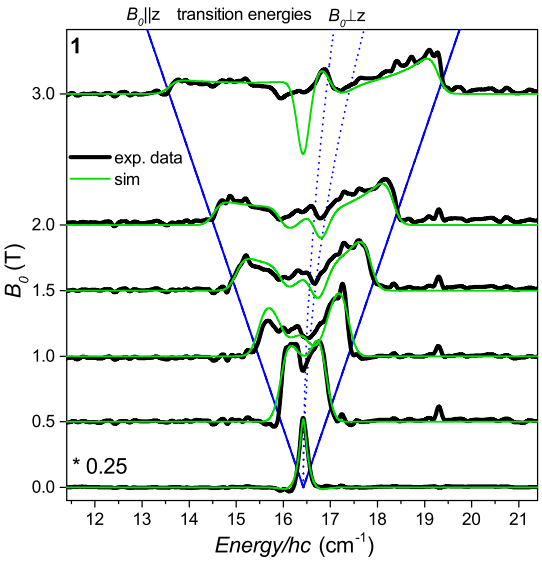

Figure 2. Field dependence of FD-FT THz-EPR spectra of **1**: $\Delta_T A$ spectra (black lines) and simulations (green lines, D/hc = 16.43 cm^{-1}, E/hc = 0.0 cm^{-1}, and g = 2.0) at different magnetic fields $\boldsymbol{B}_0$ and a fixed temperature of 5 K. The spectra are offset according to the magnetic field value and rescaled with a single factor for measurements (and simulations) with the applied field. A different scaling factor was used for the data measured without magnetic field. The calculated transition energies for $\boldsymbol{B}_0$ perpendicular (dotted) and parallel (solid) to the main molecular anisotropy axis are shown as blue lines.

DOI: 10.1021/acs.inorgchem.8b02670
Inorg. Chem. 2018, 57, 15330−15340

Its temperature dependence in the absence of the magnetic field is shown in Figure 3. At the lowest temperatures (below 7 K), the $\Delta_T A$ value could not be reliably determined because of an almost complete absorption of radiation by the sample (see Figure S1 in the Supporting Information). At higher temperatures, $\Delta_T A$ decreases with increasing temperature, which is a clear indication that the resonance originates from a ground-state transition. The position of the resonance directly provides D and E. The magnetic anisotropy is purely axial within experimental accuracy ($E/hc \lesssim 0.1$ cm^{-1}), as only one narrow resonance is observed. Furthermore, the energy position at which the maximum $\Delta_T A$ occurred decreases with increasing temperature from 16.43(2) cm^{-1} at 2.7 K to 16.27(4) cm^{-1} at 38 K (Figure 3). The reason for this shift is not immediately clear and is discussed below. No obvious trends with temperature could be observed in the line width of the feature (see Figure S2 in the Supporting Information).

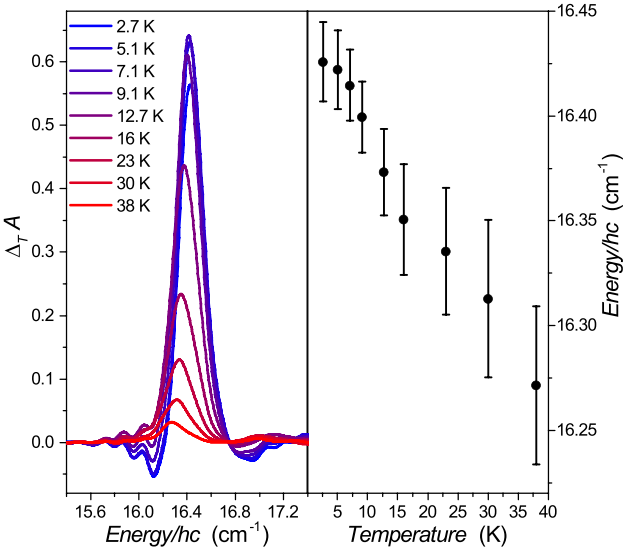

Figure 3. Temperature dependence of FD-FT THz-EPR spectra of **1**: Left: $\Delta_T A$ spectra measured without the magnetic field at different temperatures. Right: Absorbance energy (peak maximum) as a function of temperature.

Fitting the temperature dependence of χT from variable-temperature dc magnetic susceptibility measurements with the program PHI[76] and eq 1 is successful only if a positive D is assumed (Figure 1). Doing so gives the following best-fit parameters for **1**: D/hc = 14.4 cm^{-1}, E/hc = 0 cm^{-1}, and g = 2.036. Multireference ab-initio calculations within the CASSCF/NEVPT2 approach, as implemented in the ORCA software[58] (see Experimental Section for details), produce[72] a very similar temperature dependence of χT (Figure 1); however, the calculated magnetic parameters are different (D/hc = 18.7 cm^{-1}, E/hc = 0.0 cm^{-1}, and g = 2.08). Obviously, although computational methods are very helpful,[77,78] in our case, they give D and g that deviate substantially from the experimental values.

In contrast to magnetic susceptibility measurements and quantum chemical calculations, FD-FT THz-EPR is a spectroscopic technique that gives direct experimental access to the ZFS. The following magnetic parameters of **1** are obtained by simulating the field dependence of the FD-FT THz-EPR spectra, measured at a temperature of 5 K, with EasySpin[52,79,80] and eq 1: D/hc = 16.43(1) cm^{-1}, E/hc = 0.0(1) cm^{-1}, and g = 2.0(1). Only at the highest magnetic field of 3 T, the simulations deviate at around 16.4 cm^{-1} from the experimental results (see Figure 2). Although the simulated absorption at 3 T in this region is apparently too low, the agreement elsewhere is excellent. Hence, the field-induced line broadening can be assigned to Zeeman interaction between the external magnetic field and the spins of the randomly oriented molecules. The asymmetry of the spectrum at higher magnetic fields ($\Delta_T A$ being slightly larger at the high-energy end) results from powder averaging and the division method used in the data analysis (see Figure S5 in the Supporting Information). The magnetic susceptibility χT is also well reproduced with these parameters (see Figure 1). Introducing a negative D into the simulations makes the agreement with the experimental data from FD-FT THz-EPR slightly worse and much worse with those from the magnetic susceptibility measurements (see Figures S3 and S4 in the Supporting Information).

The use of two different methods of estimating the magnetic anisotropy allows us to compare their accuracy. The spectroscopic observation of the ZFS with FD-FT THz-EPR provides the highest precision given its direct nature. For a relatively wide range of D and E values, a satisfying agreement with the measured χT curve is obtained. Hence, magnetometry provides only an estimate for the magnetic anisotropy.

Quantum-chemical calculations provided a reasonable estimate for D of **1** but do not yet reach the accuracy of advanced EPR spectroscopy. Therefore, experimental methods like FD-FT THz-EPR are indispensable to benchmark calculated ZFS of transition-metal ions. A combination of experimental and calculated results allows for correlating magnetic properties and the electronic structure. In the following, a brief discussion is provided for complex **1**, details can be found in the Supporting Information. The all-electron nonrelativistic eigenstates can be expressed on the basis of molecular orbitals (which in turn are eigenstates of a one-electron solution). The d_{z^2} orbital is lowest in energy, followed by nearly degenerated d_{xy} and $d_{x^2-y^2}$. Highest in energy are the nearly degenerated d_{yz} and d_{xz} (see Supporting Information). This perfectly resembles a slightly distorted trigonal prismatic ligand environment to the Co(I) ion. Subsequently, spin−orbit interaction is introduced. To obtain parameters for eq 1, the all-electron spin−orbit ground-state triplet is projected on a spin S = 1 basis and the Hamiltonian $\hat{\mathbf{S}}\mathbf{D}\hat{\mathbf{S}}$, with the anisotropy tensor $\mathbf{D}$.[82] A coordination transformation to the ZFS frame lead to the form of eq 1. The individual contribution of the nonrelativistic states can be estimated by decomposing $\mathbf{D}$. As the individual ZFS frames are not necessarily colinear with the total ZFS frame, the individual contributions to D and E do not have to add up to the total D and E. However, the overall deviation is less than 0.6 cm^{-1} for D and 10^{-3} cm^{-1} for E, indicating that is worthwhile to analyze the individual contributions, providing a rationale for the calculated ZFS. The calculated D and E are obtained with the effective Hamiltonian approach which provides a better estimate than the perturbation theory approach. However, we will use the latter in the following for the sake of simplicity. The contribution of the nonrelativistic states to D depends on the energy difference to the ground-state and the matrix elements $\hat{\mathbf{S}}\cdot\hat{\mathbf{L}}$ of these state with the ground state.[6] The latter are best understood using group theory arguments. A perfect trigonal prismatic molecule would have D_{3h} symmetry. Although **1** has a reduced symmetry due to the second ligand sphere, it is instructive to consider the idealized symmetry for the analysis. Nonrelativistic states of **1**, assigned to the ^{3}F, ^{1}D, and ^{3}P of the free Co(I) ion,

DOI: 10.1021/acs.inorgchem.8b02670
Inorg. Chem. 2018, 57, 15330−15340

are shown in Figure 4 alongside with the assigned irreducible representation in D_{3h}. Table 2 also contains their contribution to

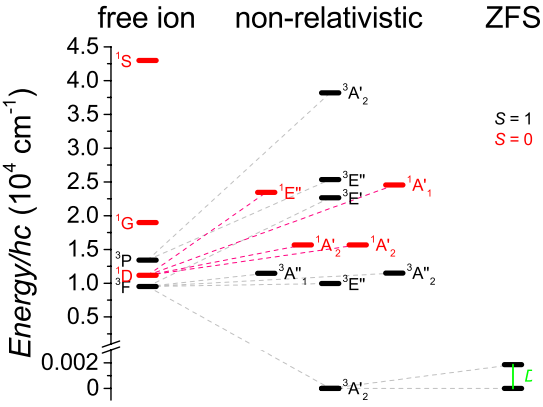

Figure 4. Splitting of energy levels according to NEVPT2/CASSCF calculations. On the left side, the d^8 energy levels of a free Co(I) ion are shown.[81] The calculated nonrelativistic energy splitting of **1** is shown in the center for states associated to ^{3}F, ^{1}D, and ^{3}P. The assigned irreducible representation in (idealized) D_{3h} symmetry is also included. The ZFS of the ground-state triplet after inclusion of spin−orbit interaction is shown on the right. Triplet, $S = 1$, and (singlet, $S = 0$) states are shown in black (red). The dashed lines are guides to the eyes, which should help to identify splittings.

Table 2. Nonrelativistic States for 1[a]

energy/hc/cm^{-1}	symmetry	contribution to D/hc/cm^{-1}
0	$^3A_2'$	0.0
9932	$^3E''$	8.2
9977		8.3
11 464	$^3A_1''$	−0.2
11 507	$^3A_2''$	0.0
15 657	$^1A_2'$	0.0
15 660	$^1A_2'$	0.0
22 596	$^3E'$	0.0
22 690		0.0
23 428	$^1E''$	−3.1
23 457		−3.1
24 541	$^1A_1'$	10.4
25 322	$^3E''$	0.0
25 399		0.0
38 206	$^3A_2$	0.0

[a]Nonrelativistic states, associated to ^{3}F, ^{1}D, and ^{3}P states of the free Co(I) ion, obtained from CASSCF/NEVPT2 calculations for molecule **1**, together with their irreducible representation in (idealized) D_{3h} symmetry and their contribution to the calculated D/hc value of 18.7 cm^{-1}.

the D value. The orbital angular momentum operators $\hat{L}_x$, $\hat{L}_y$, and $\hat{L}_z$ have the irreducible representation E″, E″, and A_2' in D_{3h} symmetry, respectively.[83] The nonrelativistic ground state has $^3A_2'$ symmetry; hence, only states with $^3E''$ and $^1A_1'$ can contribute positive to D and those with $^3A_1'$ and $^1E''$ negative.[84,85] Naturally, the lowest excited doublet contribute strongest (see Table 2). It has $^3E''$ symmetry, resulting in a positive contribution to D. The small negative contribution to D of a state with $^3A_1''$ reveals that the actual symmetry of **1** is lower than D_{3h}. Further significant contributions come from spin-flip states, that is, states with spin $S = 0$. The lowest spin-flip states do not contribute due to symmetry; however, a higher-lying $^1E''$ doublet and a $^1A_1'$ have remarkable influence on the D value. The positive contribution from the $^1A_1'$ state outweighs the negative contribution of the $^1E''$ doublet. Hence, the overall contribution of spin-flip states to D is positive. Higher-lying $S = 1$ does belong to ^{3}P (the ground state belongs to ^{3}F) and adds minor contributions to D.

The oxidation state +1 is uncommon for cobalt. The limited number of Co(I) complexes whose ZFS has been studied differ substantially in structure so that a comparison with our present complex is not meaningful. In general, D/hc values ranging from −180 to +38 cm^{-1} have been found.[32−39] Both experimentally and computationally, the rhombic anisotropy parameter E was determined here to be zero. This arises from the symmetry of the first ligation shell, where the Co(I) ion lies on a pseudo-C_3 axis (there is some slight deviation from the ideal C_3 symmetry).[57] In the case of perfect C_3 symmetry, the Hamiltonian (eq 1) would have to commute with the C_3 operator, which is only fulfilled for vanishing E.[86] Apparently, the distortions of the molecule **1** from an ideal structure with the perfect C_3 symmetry do not lead to a measurable rhombicity of the ZFS.

To further investigate the influence of structural changes on the ZFS parameters, the present study was extended to complexes **2** and **3**, which differ from **1** in the counter-ion. The small crystal sizes obtained for **2** and **3** hinder structure determination by X-ray diffraction. Hence, effects of the exchange of the counter-ion on the ligation of the Co(I) ion are probed here with FD-FT THz-EPR.

FD-FT THz EPR spectra of **2** are shown in the Supporting Information. A zero-field resonance is observed at 16.67(6) cm^{-1}, which does not shift with temperature between 2.5 and 35 K (see Figure S7). The resonance broadens under the application of a magnetic field (see Figure S6), indicating a magnetic origin. Simulations with EasySpin and eq 1 were used to determine the magnetic parameters of **2** to be D/hc = 16.67(4) cm^{-1}, E/hc = 0.0(1) cm^{-1}, and g = 2.0(1). A preferential orientation of the molecules along the magnetic field was assumed to reproduce the data recorded in the presence of a magnetic field.

In the $\Delta_T A$ spectra of **3**, several strong features were observed (see Figure S8 in the Supporting Information). Therefore, $\Delta_B A$ spectra (see Figure 5) were used to identify magnetic resonances. Two magnetic zero-field resonances were identified at 16.48(2) and 16.96(1) cm^{-1}. We will refer to them in the following as resonances 1 and 2, respectively. The application of a magnetic field broadens the resonances. Thereby, resonance 1 mainly extends to lower energies, whereas resonance 2 extends to higher energies. Additional features with varying absorption for various magnetic fields were observed at energies of approximately 16.2, 18.6, and 21.1 cm^{-1}. However, no shift in energy or broadening with magnetic field was observed. Therefore, these features are not of magnetic origin and, hence, not further considered here.

The temperature dependence of the two resonances is shown in Figure 6. Both resonances decrease in absorption with increasing temperature, indicating ground-state transitions. Further, we found that the position in energy of resonance 1 does not shift with temperature. In contrast, those of resonance 2 decreases with increasing temperature from 16.96(1) cm^{-1} at 2.4 K to 16.7(1) at 30.2 K.[87] The observation of two resonances indicates the presence of a rhombic E term. Simulations using EasySpin and eq 1 with D/hc = 16.72(2) cm^{-1}, E/hc = 0.24(3)

DOI: 10.1021/acs.inorgchem.8b02670
Inorg. Chem. 2018, 57, 15330−15340

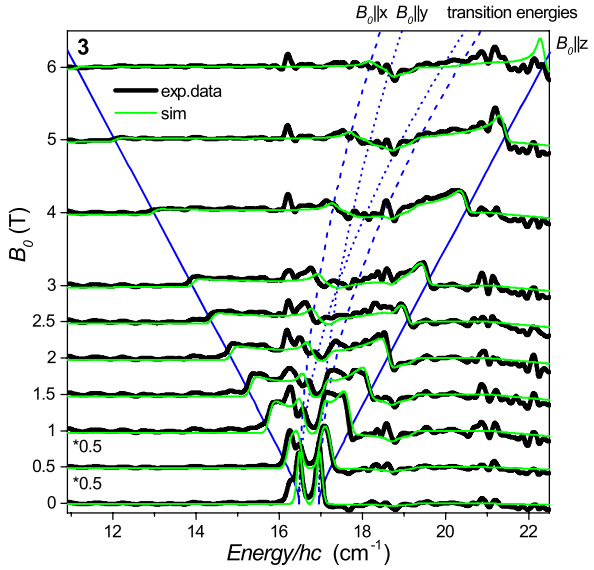

Figure 5. Field dependence of FD-FT THz-EPR spectra of **3**: $\Delta_B A$ spectra (black lines) and simulations (green lines, D/hc = 16.72 cm^{-1}, E/hc = 0.24 cm^{-1}, and g = 2.00) at different magnetic fields $\boldsymbol{B}_0$ and a fixed temperature of 2.4 K. The spectra are offset according to the magnetic field value and rescaled with a single factor for measurements (and simulations) with the applied field. A different scaling factor was used for the data measured without magnetic field. The clculated transition energies for $\boldsymbol{B}_0$ parallel to the main molecular anisotropy axes (dashed, dotted, and solid for x, y, and z axes, respectively) are shown as blue lines.

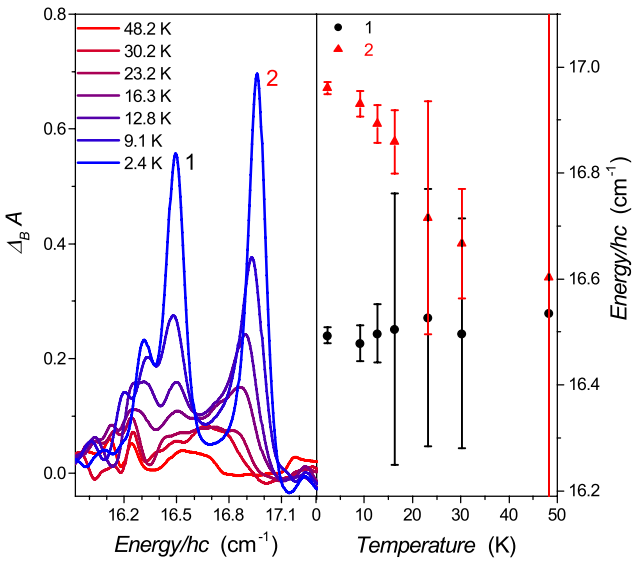

Figure 6. Temperature dependence of FD-FT THz-EPR spectra of **3**: Left: $\Delta_B A$ spectra measured at different temperatures. Right: Absorbance energies (peak maxima) as a function of temperature.

cm^{-1}, and g = 2.0(1) reproduce the field dependence of the $\Delta_B A$ spectra of **3** (see Figure 5).[88]

The variations in D values between the three Co(I) clathrochelates (see Table 3) are 1 order of magnitude above the accuracy of FD-FT THz-EPR experiments. However, they are far beyond those of SQUID magnetometry and state-of-the-art quantum chemistry methods. In addition, the lack of reliable crystal structures for **2** and **3** hinders the use of the latter. Therefore, **2** and **3** were not investigated with these techniques.

Table 3. Magnetic Anisotropy Parameters of 1, 2, and 3 Obtained in This Work by Different Experimental Methods[a]

	method	D/hc/cm^{-1}	E/hc/cm^{-1}	g
1	*CASSCF/NEVPT2*	*18.7*	*0.0*	*2.08*
	χT	14.4	0.0	2.036
	FD-FT THz-EPR	16.43(1)	0.0(1)	2.0(1)
2	FD-FT THz-EPR	16.67(4)	0.0(1)	2.0(1)
3	FD-FT THz-EPR	16.72(2)	0.24(3)	2.00(5)

[a]For comparison, computational results are also included.

Although the obtained E/D ratio of **3** of 0.014(2) is small, it is significantly different from zero. Hence, the increased rhombicity of **3** as compared to **1** and **2** was assigned to a stronger deviation from C_3 symmetry in the former case. This change may result from alterations of the Co(I) ligand environment induced by the bulkier counterion $[P(C_6H_5)_4]^+$ as compared to $[N(n\text{-}Bu)_4]^+$ or $[P(Me_2N)_4]^+$.

A further important experimental observation is that the ZFS of **1** and **3** observed by FD-FT THz-EPR decreases with increasing temperature (see Figures 3 and 6). The ZFS is often assumed to be independent of temperature. However, temperature-dependent structural changes in the environment of the paramagnetic ion could lead in turn to a temperature-dependent ZFS. This can be due to structural phase transitions,[57] lattice vibrations,[89,90] lattice expansions,[91,92] dynamic distortions,[57,93−95] dynamic Jahn−Teller effects,[96,97] or weak IMIs.[98]

If a structural phase transition would occur, the crystal packing of the Co(I) clathrochelates should change with temperature, as it was observed for a related Co(II) clathrochelate.[57] In principle, a structural phase transition could be investigated with X-ray diffraction. However, at the temperature range of our interest, this would be a challenging undertaking. A change in crystal packing may affect the structure of individual molecules because of breaking and formation of intermolecular contacts. In turn, this could affect the ZFS. However, it is expected that a structural phase transition should lead to rather abrupt changes in crystal packing. Hence, changes in ZFS should be also abrupt, which are not observed.

Another possible reason for the temperature dependence of the ZFS is dynamic distortions, similar to those reported for iron(II)[93] and nickel(II) complexes.[94] Very recently, it was observed that small structural differences in two polymorphs of a cobalt(II) clathrochelate lead to a 50% difference in D.[95] Indications for dynamic distortions should be reflected either in the bond lengths or in the shape of the thermal ellipsoids determined from X-ray diffraction. The 100 K X-ray structure of the Co(I) clathrochelate **1** is almost perfectly axial, and the thermal ellipsoid of the cobalt ion seems only slightly elongated in the direction of one of the chelate ribs (indicating some anisotropic motion at 100 K). However, as the Co(I) ion is placed on a symmetry axis, deviations in the molecular structure might be averaged out, as was recently observed for a high-spin cobalt(II) clathrochelate.[57] All of the above described complexes had an orbitally degenerate ground state, which is prone to Jahn−Teller or Renner−Teller distortions, responsible for the dynamic distortions. In contrast, the d^8 ion Co(I) in trigonal prismatic geometry has an orbitally nondegenerate ground state.

The third possible reason for a temperature-dependent ZFS is structural changes induced by lattice expansion.[91] Nothing is known about the potential interconnection between lattice dynamics and the ZFS of the Co(I) clathrochelate. However, for

DOI: 10.1021/acs.inorgchem.8b02670
Inorg. Chem. 2018, 57, 15330−15340

a similar Co(II) complex,[92] the unit cell expanded by approximately 0.1% from 30 to 60 K, proving a reasonable estimate of the thermal expansion for the Co(I) clathrochelate.

For paramagnetic centers as probes in diamagnetic matrices, weak effects of phonons on the ZFS were observed.[89,90] This was rationalized by an inherent displacement of the paramagnetic center that affects the ZFS. The temperature-dependent phonon density might therefore introduce temperature dependence in the ZFS. To assign such spin−phonon correlations in molecular compounds is currently out of reach. However, the previously observed effects were approximately of similar relative size as those reported herein for Co(I) clathrochelates **1** and **3**.

The clathrochelate ligand forms a protective cage for the Co(I) ion. Hence, IMIs are expected to be rather weak. Inspection of potential exchange pathways in the crystal structure of **1** let us consider interactions only along the crystal *b* axis (see Supporting Information). The present situation of spins $S = 1$ weakly (compared to the magnetic anisotropy) coupled solely along one axis was studied recently.[98−100] A temperature dependence of the EPR transition, as observed here, was predicted.[100] On the basis of the observed temperature dependence, we estimated a $D/|J|$ ratio between 250 and 600 for **1** (with J, the exchange interaction strength in $\hat{H}_{\text{exchange}} = J\sum_{i=0}^{\infty}\hat{S}_i \cdot \hat{S}_{i+1}$). This corresponds to $D/hc = 16.37$ cm^{-1} (16.30 cm^{-1}) and an antiferromagnetic J/hc of 0.06 cm^{-1} (0.03 cm^{-1}) for $D/|J| = 250$ (600), respectively (see Supporting Information). Remarkably, these values exceed the expected dipolar interactions (see Supporting Information) by one order of magnitude. Exchange IMIs thus emerge as a plausible reason for the temperature dependence of ZFS. In principle, the proposed chain model can be probed experimentally. However, high-field EPR on single crystals[98,100] is currently not feasible because of the too small maximum crystal sizes obtained for Co(I) clathrochelates. In an INS experiment, the dispersion, caused by the exchange interaction, of transitions can be observed. It is, however, very challenging (even in spite of recent progress in INS of molecular clusters[101−105]), as large $D/|J|$ makes this dispersion not very pronounced (see Figure S13). An obvious way to test the impact of IMIs on ZFS would be to increase the distance between the spin centers. This can be reached by experiments on a low-concentration frozen solution or by magnetic dilution with a diamagnetic analogon of the Co(I) ion. The former is challenging because of strong nonmagnetic absorption of solvents. The latter is not feasible, as the only other transition-metal ion reported to be stable in the oxidation state +1 inside a clathrochelate ligand is iron.[106]

In summary, on the basis of the currently available data, we cannot exclude any of the explanations. However, a structural phase transition or a dynamic Jahn−Teller effect are very unlikely to cause the observed temperature dependence of the ZFS. More likely reasons for the observed ZFS shift are lattice expansions, spin−phonon effects, or weak IMIs.

CONCLUSIONS

ZFS in a series of Co(I) clathrochelate was determined with high precision by advanced FD-FT THz-EPR. The complementary use of susceptibility measurements alongside with FD-FT THz-EPR for **1** allowed for an assignment of both absolute value and sign of $D/hc = +16.43(1)$ cm^{-1}. This approach also demonstrated that FD-FT THz-EPR provides much higher accuracy and reliability in the determined ZFS values than single fits to magnetic susceptibility data. The determined magnetic anisotropy is of a hard-axis type ($D > 0$) and fully axial ($E/hc = 0.0(1)$ cm^{-1}). The latter may be rationalized by the fact that the X-ray structure shows only very little deviation from a perfect C_3 symmetry. Ab initio NEVPT2/CASSCF calculations provided a reasonable estimate of the ZFS. However, they are indispensable for understanding the contribution of the electronic structure to the magnetic properties. In conjunction with symmetry arguments, the calculations allowed to rationalize the contributions to the ZFS for **1**. ZFS of **2** was found fully axial ($E/hc = 0.0(1)$ cm^{-1}) with slightly increased hard-axis anisotropy compared to **1** ($D/hc = 16.67(4)$ cm^{-1}). In contrast, slight rhombicity ($D/hc = 16.72(2)$ cm^{-1}, $E/hc = 0.24(3)$ cm^{-1}) was found for **3**, indicating distortion from the C_3 symmetry. **2** and **3** have been synthesized in the same way as **1**, but with a different counter-ion. Although these changes might seem irrelevant for the coordination sphere of the Co(I) ion, we observed an effect on the ZFS. Hence, determination of the ZFS by FD-FT THz-EPR provides a powerful probe for effects of the exchange of the counter-ion on the ligation shell of the Co(I) ion. In fact, it was the only accessible probe because of the lack of crystal structures for **2** and **3**. The superior resolution of FD-FT THz-EPR further revealed a slight temperature dependence of the Co(I) ZFS. Possible explanations include temperature-dependent structural changes, spin−phonon interactions, and weak chain-like antiferromagnetic IMIs with J of only a few per mille of D. As this phenomenon occurs in a compound with the metal ion well isolated from the environment, a further discrimination of intra- and intermolecular contributions to the magnetic properties would be of great interest. This adds another aspect that needs to be kept in mind while designing new MNMs. The observation of such subtle effects has been difficult up to now, as they require high-purity samples exhibiting narrow lines and high-end spectroscopy. We, however, expect that further progress in high-frequency EPR instrumentation will soon make them more widely accessible.

ASSOCIATED CONTENT

Supporting Information

The Supporting Information is available free of charge on the ACS Publications website at DOI: 10.1021/acs.inorgchem.8b02670.

Additional results of quantum chemical calculations; estimation of intermolecular interactions; and calculation of dipolar interaction strength between Co(I) ions (PDF)

AUTHOR INFORMATION

Corresponding Authors

*E-mail: nehrkorn@uw.edu (J.N.).
*E-mail: alexander.schnegg@cec.mpg.de (A.S.).

ORCID

Joscha Nehrkorn: 0000-0003-1156-5675
Sergey L. Veber: 0000-0002-5445-3713
Valentin V. Novikov: 0000-0002-0225-0594
Yulia V. Nelyubina: 0000-0002-9121-0040
Yan Z. Voloshin: 0000-0003-2823-6560
Stefan Stoll: 0000-0003-4255-9550

Notes

The authors declare no competing financial interest.

ACKNOWLEDGMENTS

This work has been supported and funded by Deutsche Forschungsgemeinschaft (DFG) through priority program

DOI: 10.1021/acs.inorgchem.8b02670
Inorg. Chem. 2018, 57, 15330−15340

SPP 1601, a Research Fellowship (grant no. NE 2064/1-1 FOR) to J.N., and RFBR (grant no. 16-03-00688). Participation of S.L.V. at the FD-FT THz-EPR experiment was supported by RSF (grant no. 17-13-01412). J.N. would like to thank Samuel M. Greer (National High Magnetic Field Laboratory, Tallahassee) for help with the quantum chemical calculations. The authors thank Robert Bittl (Freie Universität Berlin) for permitting experiments at the Frequency Domain Fourier Transform THz-EPR setup and Dirk Ponwitz (Helmholtz-Zentrum Berlin) for technical support.

REFERENCES

(1) Gatteschi, D.; Sessoli, R.; Villain, J. *Molecular Nanomagnets*; OUP: Oxford, 2006.
(2) Mannini, M.; Pineider, F.; Sainctavit, P.; Danieli, C.; Otero, E.; Sciancalepore, C.; Talarico, A. M.; Arrio, M.-A.; Cornia, A.; Gatteschi, D.; Sessoli, R. Magnetic Memory of a Single-Molecule Quantum Magnet Wired to a Gold Surface. *Nat. Mater.* **2009**, *8*, 194−197.
(3) Bogani, L.; Wernsdorfer, W. Molecular Spintronics Using Single-Molecule Magnets. *Nat. Mater.* **2008**, *7*, 179−186.
(4) Leuenberger, M. N.; Loss, D. Quantum Computing in Molecular Magnets. *Nature* **2001**, *410*, 789−793.
(5) Manoli, M.; Johnstone, R. D. L.; Parsons, S.; Murrie, M.; Affronte, M.; Evangelisti, M.; Brechin, E. K. A Ferromagnetic Mixed-Valent Mn Supertetrahedron: Towards Low-Temperature Magnetic Refrigeration with Molecular Clusters. *Angew. Chem., Int. Ed.* **2007**, *46*, 4456−4460.
(6) Neese, F. Zero-Field Splitting. In *Calculation of NMR and EPR Parameters*; Kaupp, M., Michael, B., Malkin, V. G., Eds.; Wiley-VCH Verlag GmbH & Co. KGaA, 2004; pp 541−564.
(7) Boča, R. Zero-Field Splitting in Metal Complexes. *Coord. Chem. Rev.* **2004**, *248*, 757−815.
(8) Schnack, J. Influence of Intermolecular Interactions on Magnetic Observables. *Phys. Rev. B* **2016**, *93*, 054421.
(9) DiVincenzo, D. P.; Bacon, D.; Kempe, J.; Burkard, G.; Whaley, K. B. Universal Quantum Computation with the Exchange Interaction. *Nature* **2000**, *408*, 339−342.
(10) Layfield, R. A.; McDouall, J. J. W.; Sulway, S. A.; Tuna, F.; Collison, D.; Winpenny, R. E. P. Influence of the N-Bridging Ligand on Magnetic Relaxation in an Organometallic Dysprosium Single-Molecule Magnet. *Chem.—Eur. J.* **2010**, *16*, 4442−4446.
(11) Liu, J.; Chen, Y.-C.; Liu, J.-L.; Vieru, V.; Ungur, L.; Jia, J.-H.; Chibotaru, L. F.; Lan, Y.; Wernsdorfer, W.; Gao, S.; Chen, X.-M.; Tong, M.-L. A Stable Pentagonal Bipyramidal Dy(III) Single-Ion Magnet with a Record Magnetization Reversal Barrier over 1000 K. *J. Am. Chem. Soc.* **2016**, *138*, 5441−5450.
(12) Blagg, R. J.; Ungur, L.; Tuna, F.; Speak, J.; Comar, P.; Collison, D.; Wernsdorfer, W.; McInnes, E. J. L.; Chibotaru, L. F.; Winpenny, R. E. P. Magnetic Relaxation Pathways in Lanthanide Single-Molecule Magnets. *Nat. Chem.* **2013**, *5*, 673−678.
(13) Colacio, E.; Ruiz, J.; Ruiz, E.; Cremades, E.; Krzystek, J.; Carretta, S.; Cano, J.; Guidi, T.; Wernsdorfer, W.; Brechin, E. K. Slow Magnetic Relaxation in a CoII-YIII Single-Ion Magnet with Positive Axial Zero-Field Splitting. *Angew. Chem., Int. Ed.* **2013**, *52*, 9130−9134.
(14) Pinkowicz, D.; Southerland, H. I.; Avendaño, C.; Prosvirin, A.; Sanders, C.; Wernsdorfer, W.; Pedersen, K. S.; Dreiser, J.; Clérac, R.; Nehrkorn, J.; Simeoni, G. G.; Schnegg, A.; Holldack, K.; Dunbar, K. R. Cyanide Single-Molecule Magnets Exhibiting Solvent Dependent Reversible "On" and "Off" Exchange Bias Behavior. *J. Am. Chem. Soc.* **2015**, *137*, 14406−14422.
(15) Vaidya, S.; Tewary, S.; Singh, S. K.; Langley, S. K.; Murray, K. S.; Lan, Y.; Wernsdorfer, W.; Rajaraman, G.; Shanmugam, M. What Controls the Sign and Magnitude of Magnetic Anisotropy in Tetrahedral Cobalt(II) Single-Ion Magnets? *Inorg. Chem.* **2016**, *55*, 9564−9578.
(16) Miyasaka, H.; Nakata, K.; Sugiura, K.-i.; Yamashita, M.; Clérac, R. A three-dimensional ferrimagnet composed of mixed-valence Mn_4 clusters linked by an $\{Mn[N(CN_2)]_6\}^{4-}$ unit. *Angew. Chem., Int. Ed.* **2004**, *43*, 707−711.
(17) Miyasaka, H.; Nakata, K.; Lecren, L.; Coulon, C.; Nakazawa, Y.; Fujisaki, T.; Sugiura, K.-i.; Yamashita, M.; Clérac, R. Two-dimensional network based on Mn_4 complex linked by dycyanamide anion: From single-molecule magnet to classical magnet behavior. *J. Am. Chem. Soc.* **2006**, *128*, 3770−3783.
(18) Yamaguchi, A.; Kusumi, N.; Ishimoto, H.; Mitamura, H.; Goto, T.; Mori, N.; Nakano, M.; Awaga, K.; Yoo, J.; Hendrickson, D. N.; Christou, G. Observation of Magnetic Transition in Quantum Nanomagnet Mn_4Br. *J. Phys. Soc. Jpn.* **2002**, *71*, 414−417.
(19) Affronte, M.; Lasjaunias, J. C.; Wernsdorfer, W.; Sessoli, R.; Gatteschi, D.; Heath, S. L.; Fort, A.; Rettori, A. Magnetic ordering in a high-spin Fe_{19} molecular nanomagnet. *Phys. Rev. B: Condens. Matter Mater. Phys.* **2002**, *66*, 064408.
(20) Boskovic, C.; Bircher, R.; Tregenna-Piggott, P. L. W.; Güdel, H. U.; Paulsen, C.; Wernsdorfer, W.; Barra, A.-L.; Khatsko, E.; Neels, A.; Stoeckli-Evans, H. Ferromagnetic and Antiferromagnetic Intermolecular Interactions in a New Family of Mn_4 Complexes with an Energy Barrier to Magnetization Reversal. *J. Am. Chem. Soc.* **2003**, *125*, 14046−14058.
(21) Wernsdorfer, W.; Aliaga-Alcalde, N.; Hendrickson, D. N.; Christou, G. Exchange-biased quantum tunnelling in a supramolecular dimer of single-molecule magnets. *Nature* **2002**, *416*, 406−409.
(22) Wernsdorfer, W.; Bhaduri, S.; Vinslava, A.; Christou, G. Landau-Zener tunneling in the presence of weak intermolecular interactions in a crystal of Mn_4 single-molecule magnets. *Phys. Rev. B: Condens. Matter Mater. Phys.* **2005**, *72*, 214429.
(23) Tiron, R.; Wernsdorfer, W.; Foguet-Albiol, D.; Aliaga-Alcalde, N.; Christou, G. Spin Quantum Tunneling via Entangled States in a Dimer of Exchange-Coupled Single-Molecule Magnets. *Phys. Rev. Lett.* **2003**, *91*, 227203.
(24) Tiron, R.; Wernsdorfer, W.; Aliaga-Alcalde, N.; Christou, G. Quantum tunneling in a three-dimensional network of exchange-coupled single-molecule magnets. *Phys. Rev. B: Condens. Matter Mater. Phys.* **2003**, *68*, 140407.
(25) Ortigoza, M. A.; Klemm, R. A.; Rahman, T. S. Effect of dipolar interactions on the magnetization of a cubic array of nanomagnets. *Phys. Rev. B: Condens. Matter Mater. Phys.* **2005**, *72*, 174416.
(26) Park, K.; Novotny, M. A.; Dalal, N. S.; Hill, S.; Rikvold, P. A. Effects of D-strain, g-strain, and dipolar interactions on EPR linewidths of the molecular magnets Fe_8 and Mn_{12}. *Phys. Rev. B: Condens. Matter Mater. Phys.* **2001**, *65*, 014426.
(27) Park, K.; Novotny, M. A.; Dalal, N. S.; Hill, S.; Rikvold, P. A. Role of dipolar and exchange interactions in the positions and widths of EPR transitions for the single-molecule magnets Fe_8 and Mn_{12}. *Phys. Rev. B: Condens. Matter Mater. Phys.* **2002**, *66*, 144409.
(28) Murrie, M. Cobalt(II) Single-Molecule Magnets. *Chem. Soc. Rev.* **2010**, *39*, 1986−1995.
(29) Craig, G. A.; Murrie, M. 3d Single-Ion Magnets. *Chem. Soc. Rev.* **2015**, *44*, 2135−2147.
(30) Suturina, E. A.; Nehrkorn, J.; Zadrozny, J. M.; Liu, J.; Atanasov, M.; Weyhermüller, T.; Maganas, D.; Hill, S.; Schnegg, A.; Bill, E.; Long, J. R.; Neese, F. Magneto-Structural Correlations in Pseudotetrahedral Forms of the $[Co(SPh)_4]^{2-}$ Complex Probed by Magnetometry, MCD Spectroscopy, Advanced EPR Techniques, and ab Initio Electronic Structure Calculations. *Inorg. Chem.* **2017**, *56*, 3102−3118.
(31) Ziegenbalg, S.; Hornig, D.; Görls, H.; Plass, W. Cobalt(II)-Based Single-Ion Magnets with Distorted Pseudotetrahedral $[N_2O_2]$ Coordination: Experimental and Theoretical Investigations. *Inorg. Chem.* **2016**, *55*, 4047−4058.
(32) Meier, S. C.; Holz, A.; Kulenkampff, J.; Schmidt, A.; Kratzert, D.; Himmel, D.; Schmitz, D.; Scheidt, E.-W.; Scherer, W.; Bülow, C.; Timm, M.; Lindblad, R.; Akin, S. T.; Zamudio-Bayer, V.; von Issendorff, B.; Duncan, M. A.; Lau, J. T.; Krossing, I. Access to the Bis-benzene Cobalt(I) Sandwich Cation and its Derivatives: Synthons for a "Naked" Cobalt(I) Source? *Angew. Chem., Int. Ed.* **2018**, *57*, 9310−9314.
(33) Zhao, P.; Brown, Z.; Fettinger, J. C.; Grandjean, F.; Long, G. J.; Power, P. P. Synthesis and Structural Characterization of a Dimeric

DOI: 10.1021/acs.inorgchem.8b02670
Inorg. Chem. 2018, 57, 15330−15340

Cobalt(I) Homoleptic Alkyl and an Iron(II) Alkyl Halide Complex. *Organometallics* **2014**, *33*, 1917−1920.
(34) Lin, C.-Y.; Fettinger, J. C.; Grandjean, F.; Long, G. J.; Power, P. P. Synthesis, Structure, and Magnetic and Electrochemical Properties of Quasi-Linear and Linear Iron(I), Cobalt(I), and Nickel(I) Amido Complexes. *Inorg. Chem.* **2014**, *53*, 9400−9406.
(35) Al-Afyouni, M. H.; Suturina, E.; Pathak, S.; Atanasov, M.; Bill, E.; DeRosha, D. E.; Brennessel, W. W.; Neese, F.; Holland, P. L. Spin Isomers and Ligand Isomerization in a Three-Coordinate Cobalt(I) Carbonyl Complex. *J. Am. Chem. Soc.* **2015**, *137*, 10689−10699.
(36) O'Hare, D.; Rai-Chaudhuri, A.; Murphy, V. Synthesis and Magnetic Properties of 1:1 Salts Containing the Bis(η_6-Hexamethylbenzene)Cobalt Cation. *J. Chem. Soc., Dalton Trans.* **1993**, 3071−3074.
(37) Rose, M. J.; Bellone, D. E.; Di Bilio, A. J.; Gray, H. B. Spectroscopic and magnetic properties of an iodo CoI tripodal phosphine complex. *Dalton Trans.* **2012**, *41*, 11788−11797.
(38) Krzystek, J.; Ozarowski, A.; Zvyagin, S. A.; Telser, J. High Spin Co(I): High-Frequency and -Field EPR Spectroscopy of $CoX(PPh_3)_3$ (X = Cl, Br). *Inorg. Chem.* **2012**, *51*, 4954−4964.
(39) England, J.; Bill, E.; Weyhermüller, T.; Neese, F.; Atanasov, M.; Wieghardt, K. Molecular and Electronic Structures of Homoleptic Six-Coordinate Cobalt(I) Complexes of 2,2′:6′,2″-Terpyridine, 2,2′-Bipyridine, and 1,10-Phenanthroline. An Experimental and Computational Study. *Inorg. Chem.* **2015**, *54*, 12002−12018.
(40) Voloshin, Y. Z.; Kostromina, N. A.; Krämer, R. *Clathrochelates: Synthesis, Structure and Properties*; Elsevier, 2002.
(41) Voloshin, Y. Z.; Varzatskii, O. A.; Vorontsov, I. I.; Antipin, M. Y. Tuning a Metal's Oxidation State: the Potential of Clathrochelate Systems. *Angew. Chem., Int. Ed.* **2005**, *44*, 3400−3402.
(42) Novikov, V. V.; Pavlov, A. A.; Nelyubina, Y. V.; Boulon, M.-E.; Varzatskii, O. A.; Voloshin, Y. Z.; Winpenny, R. E. P. A Trigonal Prismatic Mononuclear Cobalt(II) Complex Showing Single-Molecule Magnet Behavior. *J. Am. Chem. Soc.* **2015**, *137*, 9792−9795.
(43) Krzystek, J.; Telser, J. Measuring Giant Anisotropy in Paramagnetic Transition Metal Complexes with Relevance to Single-Ion Magnetism. *Dalton Trans.* **2016**, *45*, 16751−16763.
(44) Moseley, D. H.; Stavretis, S. E.; Thirunavukkuarasu, K.; Ozerov, M.; Cheng, Y.; Daemen, L. L.; Ludwig, J.; Lu, Z.; Smirnov, D.; Brown, C. M.; Pandey, A.; Ramirez-Cuesta, A. J.; Lamb, A. C.; Atanasov, M.; Bill, E.; Neese, F.; Xue, Z.-L. Spin - phonon couplings in transition metal complexes with slow magnetic relaxation. *Nat. Commun.* **2018**, *9*, 2572.
(45) Novitchi, G.; Jiang, S.; Shova, S.; Rida, F.; Hlavička, I.; Orlita, M.; Wernsdorfer, W.; Hamze, R.; Martins, C.; Suaud, N.; Guihéry, N.; Barra, A.-L.; Train, C. From Positive to Negative Zero-Field Splitting in a Series of Strongly Magnetically Anisotropic Mononuclear Metal Complexes. *Inorg. Chem.* **2017**, *56*, 14809−14822.
(46) Palacios, M. A.; Nehrkorn, J.; Suturina, E. A.; Ruiz, E.; Gómez-Coca, S.; Holldack, K.; Schnegg, A.; Krzystek, J.; Moreno, J. M.; Colacio, E. Analysis of Magnetic Anisotropy and the Role of Magnetic Dilution in Triggering Single-Molecule Magnet (SMM) Behavior in a Family of CoII YIII Dinuclear Complexes with Easy-Plane Anisotropy. *Chem.—Eur. J.* **2017**, *23*, 11649−11661.
(47) Rasheed, W.; Draksharapu, A.; Banerjee, S.; Young, V. G., Jr.; Fan, R.; Guo, Y.; Ozerov, M.; Nehrkorn, J.; Krzystek, J.; Telser, J.; Que, L. Crystallographic evidence for a sterically induced ferryl tilt in a non-heme oxoiron(IV) complex that makes it a better oxidant. *Angew. Chem., Int. Ed.* **2018**, *57*, 9387−9391.
(48) Bucinsky, L.; Breza, M.; Lee, W.-T.; Hickey, A. K.; Dickie, D. A.; Nieto, I.; DeGayner, J. A.; Harris, T. D.; Meyer, K.; Krzystek, J.; Ozarowski, A.; Nehrkorn, J.; Schnegg, A.; Holldack, K.; Herber, R. H.; Telser, J.; Smith, J. M. Spectroscopic and Computational Studies of Spin States of Iron(IV) Nitrido and Imido Complexes. *Inorg. Chem.* **2017**, *56*, 4751−4768.
(49) van Slageren, J. New Directions in Electron Paramagnetic Resonance Spectroscopy on Molecular Manomagnets. In *EPR Spectroscopy: Applications in Chemistry and Biology*; Drescher, M., Jeschke, G., Eds.; Springer: Berlin, Heidelberg, 2012; pp 199−234.
(50) Marx, R.; Moro, F.; Dörfel, M.; Ungur, L.; Waters, M.; Jiang, S. D.; Orlita, M.; Taylor, J.; Frey, W.; Chibotaru, L. F.; van Slageren, J. Spectroscopic Determination of Crystal Field Splittings in Lanthanide Double Deckers. *Chem. Sci.* **2014**, *5*, 3287−3293.
(51) Rechkemmer, Y.; Breitgoff, F. D.; van der Meer, M.; Atanasov, M.; Hakl, M.; Orlita, M.; Neugebauer, P.; Neese, F.; Sarkar, B.; van Slageren, J. A Four-Coordinate Cobalt(II) Single-Ion Magnet with Coercivity and a Very High Energy Barrier. *Nat. Commun.* **2016**, *7*, 10467.
(52) Nehrkorn, J.; Telser, J.; Holldack, K.; Stoll, S.; Schnegg, A. Simulating Frequency-Domain Electron Paramagnetic Resonance: Bridging the Gap between Experiment and Magnetic Parameters for High-Spin Transition-Metal Ion Complexes. *J. Phys. Chem. B* **2015**, *119*, 13816−13824.
(53) Schnegg, A.; Behrends, J.; Lips, K.; Bittl, R.; Holldack, K. Frequency Domain Fourier Transform THz-EPR on Single Molecule Magnets using Coherent Synchrotron Radiation. *Phys. Chem. Chem. Phys.* **2009**, *11*, 6820−6825.
(54) Dreiser, J.; Pedersen, K. S.; Schnegg, A.; Holldack, K.; Nehrkorn, J.; Sigrist, M.; Tregenna-Piggott, P.; Mutka, H.; Weihe, H.; Mironov, V. S.; Bendix, J.; Waldmann, O. Three-Axis Anisotropic Exchange Coupling in the Single-Molecule Magnets $NEt_4[Mn_2III(5\text{-}Brsalen)_2(MeOH)_2M^{III}(CN)_6]$ (M=Ru, Os). *Chem.—Eur. J.* **2013**, *19*, 3693−3701.
(55) Dreiser, J.; Schnegg, A.; Holldack, K.; Pedersen, K. S.; Schau-Magnussen, M.; Nehrkorn, J.; Tregenna-Piggott, P.; Mutka, H.; Weihe, H.; Bendix, J.; Waldmann, O. Frequency-Domain Fourier-Transform Terahertz Spectroscopy of the Single-Molecule Magnet (NEt^4)-$[Mn_2(5\text{-}Brsalen)_2(MeOH)_2Cr(CN)_6]$. *Chem.—Eur. J.* **2011**, *17*, 7492−7498.
(56) Pedersen, K. S.; Dreiser, J.; Nehrkorn, J.; Gysler, M.; Schau-Magnussen, M.; Schnegg, A.; Holldack, K.; Bittl, R.; Piligkos, S.; Weihe, H.; Tregenna-Piggott, P.; Waldmann, O.; Bendix, J. A Linear Single-Molecule Magnet Based on $[Ru^{III}(CN)_6]^{3-}$. *Chem. Commun.* **2011**, *47*, 6918−6920.
(57) Voloshin, Y. Z.; Varzatskii, O. A.; Novikov, V. V.; Strizhakova, N. G.; Vorontsov, I. I.; Vologzhanina, A. V.; Lyssenko, K. A.; Romanenko, G. V.; Fedin, M. V.; Ovcharenko, V. I.; Bubnov, Y. N. Tris-Dioximate Cobalt(I,II,III) Clathrochelates: Stabilization of Different Oxidation and Spin States of an Encapsulated Metal Ion by Ribbed Functionalization. *Eur. J. Inorg. Chem.* **2010**, *2010*, 5401−5415.
(58) Neese, F. The ORCA Program System. *Wiley Interdiscip. Rev.: Comput. Mol. Sci.* **2012**, *2*, 73−78.
(59) Perdew, J. P.; Burke, K.; Ernzerhof, M. Generalized Gradient Approximation Made Simple. *Phys. Rev. Lett.* **1996**, *77*, 3865−3868.
(60) van Wüllen, C. Molecular Density Functional Calculations in the Regular Relativistic Approximation: Method, Application to Coinage Metal Diatomics, Hydrides, Fluorides and Chlorides, and Comparison with First-Order Relativistic Calculations. *J. Chem. Phys.* **1998**, *109*, 392−399.
(61) Pantazis, D. A.; Chen, X.-Y.; Landis, C. R.; Neese, F. All-Electron Scalar Relativistic Basis Sets for Third-Row Transition Metal Atoms. *J. Chem. Theory Comput.* **2008**, *4*, 908−919.
(62) Weigend, F.; Ahlrichs, R. Balanced Basis Sets of Split Valence, Triple Zeta Valence and Quadruple Zeta Valence Quality for H to Rn: Design and Assessment of Accuracy. *Phys. Chem. Chem. Phys.* **2005**, *7*, 3297−3305.
(63) Stoychev, G. L.; Auer, A. A.; Neese, F. Automatic Generation of Auxiliary Basis Sets. *J. Chem. Theory Comput.* **2017**, *13*, 554−562.
(64) Hess, B. A. Relativistic electronic-structure calculations employing a two-component no-pair formalism with external-field projection operators. *Phys. Rev. A* **1986**, *33*, 3742−3748.
(65) Andersson, K.; Malmqvist, P. A.; Roos, B. O.; Sadlej, A. J.; Wolinski, K. Second-order perturbation theory with a CASSCF reference function. *J. Phys. Chem.* **1990**, *94*, 5483−5488.
(66) Malmqvist, P.-Å.; Roos, B. O. The CASSCF state interaction method. *Chem. Phys. Lett.* **1989**, *155*, 189−194.

DOI: 10.1021/acs.inorgchem.8b02670
Inorg. Chem. 2018, 57, 15330−15340

(67) Andersson, K.; Malmqvist, P. Å.; Roos, B. O. Second-order perturbation theory with a complete active space self-consistent field reference function. *J. Chem. Phys.* **1992**, *96*, 1218−1226.
(68) Angeli, C.; Cimiraglia, R.; Malrieu, J.-P. n-electron valence state perturbation theory: A spinless formulation and an efficient implementation of the strongly contracted and of the partially contracted variants. *J. Chem. Phys.* **2002**, *117*, 9138−9153.
(69) Angeli, C.; Cimiraglia, R.; Malrieu, J.-P. N-electron valence state perturbation theory: a fast implementation of the strongly contracted variant. *Chem. Phys. Lett.* **2001**, *350*, 297−305.
(70) Angeli, C.; Bories, B.; Cavallini, A.; Cimiraglia, R. Third-order multireference perturbation theory: The n-electron valence state perturbation-theory approach. *J. Chem. Phys.* **2006**, *124*, 054108.
(71) Angeli, C.; Cimiraglia, R.; Evangelisti, S.; Leininger, T.; Malrieu, J.-P. Introduction of n-electron valence states for multireference perturbation theory. *J. Chem. Phys.* **2001**, *114*, 10252−10264.
(72) Atanasov, M.; Ganyushin, D.; Pantazis, D. A.; Sivalingam, K.; Neese, F. Detailed Ab Initio First-Principles Study of the Magnetic Anisotropy in a Family of Trigonal Pyramidal Iron(II) Pyrrolide Complexes. *Inorg. Chem.* **2011**, *50*, 7460−7477.
(73) Nehrkorn, J.; Martins, B. M.; Holldack, K.; Stoll, S.; Dobbek, H.; Bittl, R.; Schnegg, A. Zero-Field Splittings in metHb and metMb with Aquo and Fluoro Ligands: a FD-FT THz-EPR Study. *Mol. Phys.* **2013**, *111*, 2696−2707.
(74) Nehrkorn, J.; Holldack, K.; Bittl, R.; Schnegg, A. Recent progress in synchrotron-based frequency-domain Fourier-transform THz-EPR. *J. Magn. Reson.* **2017**, *280*, 10−19.
(75) Abo-Bakr, M.; Feikes, J.; Holldack, K.; Kuske, P.; Peatman, W. B.; Schade, U.; Wüstefeld, G.; Hübers, H.-W. Brilliant, Coherent Far-Infrared (THz) Synchrotron Radiation. *Phys. Rev. Lett.* **2003**, *90*, 094801.
(76) Chilton, N. F.; Anderson, R. P.; Turner, L. D.; Soncini, A.; Murray, K. S. PHI: A powerful new program for the analysis of anisotropic monomeric and exchange-coupled polynuclear d- and f-block complexes. *J. Comput. Chem.* **2013**, *34*, 1164−1175.
(77) Retegan, M.; Cox, N.; Pantazis, D. A.; Neese, F. A First-Principles Approach to the Calculation of the On-Site Zero-Field Splitting in Polynuclear Transition Metal Complexes. *Inorg. Chem.* **2014**, *53*, 11785−11793.
(78) Atanasov, M.; Aravena, D.; Suturina, E.; Bill, E.; Maganas, D.; Neese, F. First Principles Approach to the Electronic Structure, Magnetic Anisotropy and Spin Relaxation in Mononuclear 3d-Transition Metal Single Molecule Magnets. *Coord. Chem. Rev.* **2015**, *289*−*290*, 177−214.
(79) Nehrkorn, J.; Schnegg, A.; Holldack, K.; Stoll, S. General Magnetic Transition Dipole Moments for Electron Paramagnetic Resonance. *Phys. Rev. Lett.* **2015**, *114*, 010801.
(80) Stoll, S.; Schweiger, A. EasySpin, a Comprehensive Software Package for Spectral Simulation and Analysis in EPR. *J. Magn. Reson.* **2006**, *178*, 42−55.
(81) Kramida, A.; Ralchenko, Y.; Reader, J.; NIST ASD Team. *NIST Atomic Spectra Database*, ver. 5.5.6, [Online]. Available: https://physics.nist.gov/asd; National Institute of Standards and Technology: Gaithersburg, MD, Oct 18, 2018.
(82) Maurice, R.; Bastardis, R.; Graaf, C.; Suaud, N.; Mallah, T.; Guihéry, N. Universal theoretical approach to extract anisotropic spin hamiltonians. *J. Chem. Theory Comput.* **2009**, *5*, 2977−2984.
(83) Atkins, P.; Child, M.; Phillips, C. *Tables for Group Theory*; Oxford University Press, 1978.
(84) Ganyushin, D.; Neese, F. A fully variational spin-orbit coupled complete active space self-consistent field approach: Application to electron paramagnetic resonance g-tensors. *J. Chem. Phys.* **2013**, *138*, 104113.
(85) Gomez-Coca, S.; Cremades, E.; Aliaga-Alcalde, N.; Ruiz, E. Mononuclear single-molecule magnets: tailoring the magnetic anisotropy of first-row transition-metal complexes. *J. Am. Chem. Soc.* **2013**, *135*, 7010−7018.
(86) Prather, J. Atomic Energy Levels in Crystals. In *Atomic Energy Levels in Crystals Nr. 19*; U.S. Department of Commerce, National Bureau of Standards, 1961.
(87) Due to the large uncertainty of the position in energy at 48 K this value is not considered here.
(88) Simulations with two species with slightly different D/hc and zero E/hc do reproduce the spectrum at zero field. However, in contrast to experiment, the broadening with magnetic field would be symmetric.
(89) Zheng, W.-C.; Wu, S.-Y. Theoretical Studies of the Temperature Dependence of Zero-Field Splitting of Cr^{3+} Centers in Ruby. *Phys. Rev. B: Condens. Matter Mater. Phys.* **1996**, *54*, 1117−1122.
(90) Shrivastava, K. N. Lattice Dynamic Effects in Electron Paramagnetic Resonance. *Phys. Rep.* **1975**, *20*, 137−227.
(91) Owens, F. EPR of Transition Ions as a Probe of Structural Changes. In *Magnetic Resonance of Phase Transitions*; Owens, F. J., Poole, C. P., Farach, H. A., Eds.; Academic Press, 1979; Chapter 6, pp 291−330.
(92) Novikov, V. V.; Ananyev, I. V.; Pavlov, A. A.; Fedin, M. V.; Lyssenko, K. A.; Voloshin, Y. Z. Spin-Crossover Anticooperativity Induced by Weak Intermolecular Interactions. *J. Phys. Chem. Lett.* **2014**, *5*, 496−500.
(93) Atanasov, M.; Zadrozny, J. M.; Long, J. R.; Neese, F. A Theoretical Analysis of Chemical Bonding, Vibronic Coupling, and Magnetic Anisotropy in Linear Iron(II) Complexes with Single-Molecule Magnet Behavior. *Chem. Sci.* **2013**, *4*, 139−156.
(94) Ruamps, R.; Maurice, R.; Batchelor, L.; Boggio-Pasqua, M.; Guillot, R.; Barra, A. L.; Liu, J.; Bendeif, E.-E.; Pillet, S.; Hill, S.; Mallah, T.; Guihéry, N. Giant Ising-Type Magnetic Anisotropy in Trigonal Bipyramidal Ni(II) Complexes: Experiment and Theory. *J. Am. Chem. Soc.* **2013**, *135*, 3017−3026.
(95) Pavlov, A. A.; Nelyubina, Y. V.; Kats, S. V.; Penkova, L. V.; Efimov, N. N.; Dmitrienko, A. O.; Vologzhanina, A. V.; Belov, A. S.; Voloshin, Y. Z.; Novikov, V. V. Polymorphism in a Cobalt-Based Single-Ion Magnet Tuning Its Barrier to Magnetization Relaxation. *J. Phys. Chem. Lett.* **2016**, *7*, 4111−4116.
(96) Dobe, C.; Andres, H.-P.; Tregenna-Piggott, P. L. W.; Mossin, S.; Weihe, H.; Janssen, S. Variable temperature inelastic neutron scattering study of chromium (II) Tutton salt: manifestation of the $^5E\otimes e$ Jahn-Teller effect. *Chem. Phys. Lett.* **2002**, *362*, 387−396.
(97) Tregenna-Piggott, P. L. W.; Weihe, H.; Barra, A.-L. High-Field, Multifrequency EPR Study of the $[Mn(OH_2)_6]^{3+}$ Cation: Influence of π-Bonding on the Ground State Zero-Field-Splitting Parameters. *Inorg. Chem.* **2003**, *42*, 8504−8508.
(98) Psaroudaki, C.; Zvyagin, S. A.; Krzystek, J.; Paduan-Filho, A.; Zotos, X.; Papanicolaou, N. Magnetic Excitations in the Spin-1 Anisotropic Antiferromagnet $NiCl_2$-$4SC(NH_2)_2$. *Phys. Rev. B: Condens. Matter Mater. Phys.* **2012**, *85*, 014412.
(99) Papanicolaou, N.; Spathis, P. Quantum Spin-1 Chains with Strong Planar Anisotropy. *J. Phys.: Condens. Matter* **1990**, *2*, 6575−6591.
(100) Papanicolaou, N.; Orendáčová, A.; Orendáč, M. Electron-Spin Resonance in Spin-1 Planar Magnetic Chains. *Phys. Rev. B: Condens. Matter Mater. Phys.* **1997**, *56*, 8786−8798.
(101) Nehrkorn, J.; Mukherjee, S.; Stuiber, S.; Mutka, H.; Strässle, T.; Christou, G.; Waldmann, O. Ferromagnetic Cluster Spin Waves in Molecular Disks Studied by Inelastic Neutron Scattering. *Phys. Rev. B: Condens. Matter Mater. Phys.* **2012**, *86*, 134417.
(102) Ummethum, J.; Nehrkorn, J.; Mukherjee, S.; Ivanov, N. B.; Stuiber, S.; Strässle, T.; Tregenna-Piggott, P. L. W.; Mutka, H.; Christou, G.; Waldmann, O.; Schnack, J. Discrete Antiferromagnetic Spin-Wave Excitations in the Giant Ferric Wheel Fe_{18}. *Phys. Rev. B: Condens. Matter Mater. Phys.* **2012**, *86*, 104403.
(103) Baker, M. L.; Guidi, T.; Carretta, S.; Ollivier, J.; Mutka, H.; Güdel, H. U.; Timco, G. A.; McInnes, E. J. L.; Amoretti, G.; Winpenny, R. E. P.; Santini, P. Spin Dynamics of Molecular Nanomagnets Unravelled at Atomic Scale by Four-Dimensional Inelastic Neutron Scattering. *Nat. Phys.* **2012**, *8*, 906−911.
(104) Kofu, M.; Yamamuro, O.; Kajiwara, T.; Yoshimura, Y.; Nakano, M.; Nakajima, K.; Ohira-Kawamura, S.; Kikuchi, T.; Inamura, Y.

DOI: 10.1021/acs.inorgchem.8b02670
Inorg. Chem. 2018, 57, 15330−15340

Hyperfine Structure of Magnetic Excitations in a Tb-based Single-Molecule Magnet Studied by High-Resolution Neutron Spectroscopy. *Phys. Rev. B: Condens. Matter Mater. Phys.* **2013**, *88*, 064405.
(105) Chiesa, A.; Guidi, T.; Carretta, S.; Ansbro, S.; Timco, G. A.; Vitorica-Yrezabal, I.; Garlatti, E.; Amoretti, G.; Winpenny, R. E. P.; Santini, P. Magnetic Exchange Interactions in the Molecular Nanomagnet Mn 12. *Phys. Rev. Lett.* **2017**, *119*, 217202.
(106) Voloshin, Y. Z.; Novikov, V. V.; Nelyubina, Y. V.; Belov, A. S.; Roitershtein, D. M.; Savitsky, A.; Mokhir, A.; Sutter, J.; Miehlich, M. E.; Meyer, K. Synthesis and characterization of an Fe(I) cage complex with high stability towards strong H-acids. *Chem. Commun.* **2018**, *54*, 3436–3439.

DOI: 10.1021/acs.inorgchem.8b02670
Inorg. Chem. 2018, 57, 15330–15340